Magnetic field-temperature phase diagram of multiferroic $[(CH_3)_2NH_2]Mn(HCOO)_3$

A. J. Clune,[1] K. D. Hughey,[1] C. Lee,[2,3] N. Abhyankar,[4,5,6] X. Ding,[7] N. S. Dalal,[4,5] M.-H. Whangbo,[2] J. Singleton,[7] and J. L. Musfeldt[1,8]

[1]*Department of Chemistry, University of Tennessee, Knoxville, Tennessee 37996, USA*
[2]*Department of Chemistry, North Carolina State University, Raleigh, North Carolina 27695, USA*
[3]*Department of Chemistry, Pohang University of Science and Technology, Pohang 37673, Korea*
[4]*Department of Chemistry and Biochemistry, Florida State University, Tallahassee, Florida 32306, USA*
[5]*National High Magnetic Field Laboratory, Tallahassee, Florida 32310, USA*
[6]*Center for Nanoscale Science and Technology, National Institute of Standards and Technology, Gaithersburg, Maryland 20878, USA*
[7]*National High Magnetic Field Laboratory, Los Alamos National Laboratory, Los Alamos, New Mexico 87545, USA*
[8]*Department of Physics and Astronomy, University of Tennessee, Knoxville, Tennessee 37996, USA*

(Received 10 July 2017; revised manuscript received 23 August 2017; published 18 September 2017)

We combined pulsed field magnetization and first-principles spin-density calculations to reveal the magnetic field-temperature phase diagram and spin state character in multiferroic $[(CH_3)_2NH_2]Mn(HCOO)_3$. Despite similarities with the rare earth manganites, the phase diagram is analogous to other Mn-based quantum magnets with a 0.31 T spin flop, a 15.3 T transition to the fully polarized state, and short-range correlations that persist above the ordering temperature. The experimentally accessible saturation field opens the door to exploration of the high-field phase.

DOI: 10.1103/PhysRevB.96.104424

I. INTRODUCTION

Antiferromagnets provide a flexible platform for the exploration of magnetically driven phase transitions. Examples include the classic spin flop [1–6], magnetic saturation transitions [7–9], and those with a sequence of metamagnetic, helical, and nanopantograph spin states [10–12]. The emergent class of tunable multiferroics with chemical formula $[(CH_3)_2NH_2]M(HCOO)_3$ ($M = Mn^{2+}$, Fe^{2+}, Ni^{2+}, Co^{2+}) provides a number of exciting opportunities in this regard. The Mn analog $[(CH_3)_2NH_2]Mn(HCOO)_3$ is ferroelectric below $T_C = 185$ K with polarization $P = 1.5$ μC/cm^2. It is also a weakly canted antiferromagnet below $T_N = 8.5$ K with an 0.08° canting angle [13,14]. Cross coupling between the electric and magnetic orders has been observed [15–18], and low-temperature phase separation leads to quantum tunneling of the magnetization [19]. Figure 1 displays the crystal structure of this compound and summarizes the aforementioned energy scales. The Mn^{2+} centers are connected with formate superexchange ligands with $J = -0.64$ K [20]. Dimethylammonium resides inside the anion pocket and is disordered (ordered) above (below) T_C. Surprisingly and counterintuitively, polarization is enhanced in magnetic field at temperatures well above T_N [16]. This dovetails with a recent report of sizable magnetoelectric coupling at elevated temperatures [21]. These findings suggest that there may be a magnetically driven transition at higher fields—beyond the phase space that has been thus far explored [18,22]. Other perovskitelike materials including the rare earth manganites also sport exotic phase diagrams [23], providing additional motivation for measurements of $[(CH_3)_2NH_2]Mn(HCOO)_3$ under external stimuli [24].

In order to explore the spin behavior of a model metal-organic multiferroic, we measured the magnetization of $[(CH_3)_2NH_2]Mn(HCOO)_3$ in pulsed fields up to 65 T and temperatures down to 0.37 K. The magnetic field-temperature (B-T) phase diagram developed from these data reveals a spin flop at 0.31 T and a transition to the fully saturated state at 15.3 T. The overall character of the B-T phase diagram and the in-phase → out-of-phase nature of the calculated spin-density pattern that accompanies the transition to the fully polarized magnetic state is reminiscent of other molecule-based quantum magnets like $Mn[N(CN)_2]_2$ and $MnCl_2(urea)_2$ [25,26], although in this system, we have not only an adaptable framework but also a mechanism for multiferroic behavior. In contrast to the antiferromagnetic rare earth manganites, the energy scales are smaller which makes the high-field phase

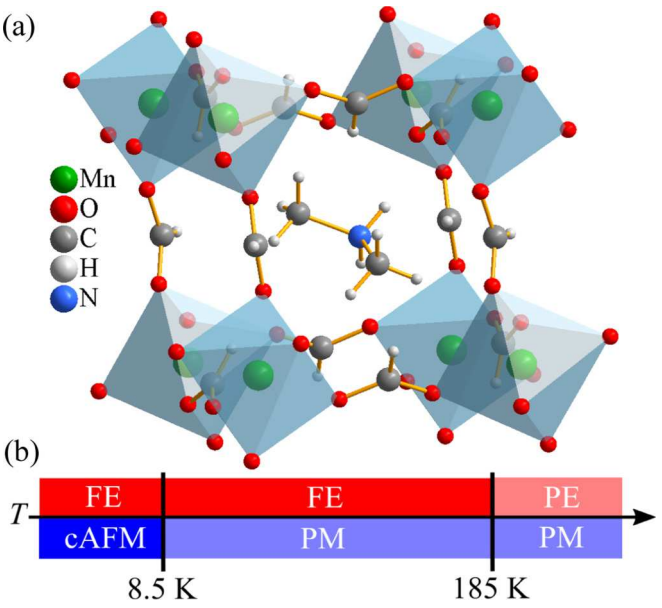

FIG. 1. (a) Crystal structure of $[(CH_3)_2NH_2]Mn(HCOO)_3$ in the low-temperature phase [20]. (b) Schematic depicting the electric and magnetic transitions that occur in this compound. (FE = ferroelectric, PE = paraelectric, cAFM = canted antiferromagnetic, and PM = paramagnetic).

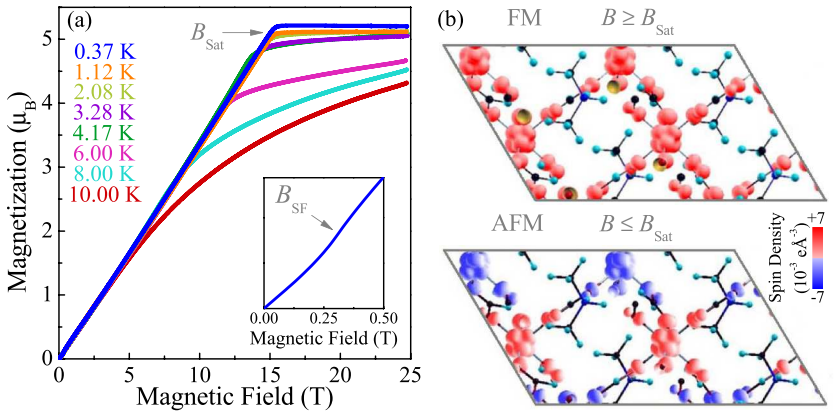

FIG. 2. (a) High-field magnetization of $[(CH_3)_2NH_2]Mn(HCOO)_3$ at temperatures above and below the 8.5 K Néel transition. The spin flop takes place at 0.31 T, and the base temperature magnetization saturates at 15.3 T. The inset shows a closeup view in the vicinity of the spin-flop transition. (b) Calculated spin density in the antiferromagnetic and ferromagnetic states of $[(CH_3)_2NH_2]Mn(HCOO)_3$. The sign of the spin density is given by the color bar.

accessible with laboratory-based magnets. This facilitates development of the full phase diagram and opens the door to deeper exploration of this system. Residual magnetization above the 8.5 K magnetic ordering temperature suggests the importance of short-range interactions, findings that we discuss in terms of magnetoelectric coupling above T_N [16,21].

II. METHODS

Polycrystalline $[(CH_3)_2NH_2]Mn(HCOO)_3$ was prepared by solvothermal reaction techniques as described previously [13,27]. Magnetization measurements were performed using a 65 T short-pulse magnet at the National High Magnetic Field Laboratory in Los Alamos using a 1.5 mm bore, 1.5 mm long, 1500 turn compensated-coil susceptometer, constructed from 50 gauge high-purity copper wire. The sample was loaded into a 1.3 mm diameter ampoule that moves in and out of the coil. The signal voltage V when the sample is in the coil is proportional to dM/dt, where t is time. M is evaluated via numerical integration. Accurate values of M were obtained by subtracting empty coil data from data measured when the sample is present, under identical conditions. Temperature was controlled with a ^{3}He system obtaining temperatures down to 0.37 K. An induced voltage in a ten-turn coil, calibrated by observing the de Haas–van Alphen oscillations of the belly orbits of the copper coils of the susceptometer, is integrated to obtain the measured field B. In addition to full field pulses, we carried out 4 and 25 T shots to better resolve the spin flop and saturation. The critical fields (B_{SF} and B_{Sat}) were determined using first derivative techniques. The pulsed field magnetization values were calibrated against measurements on a transparent single crystal with cuboidal shape in a 14 T dc magnet using a vibrating sample magnetometer.

Electronic structures for the antiferromagnetic and ferromagnetic states of $[(CH_3)_2NH_2]Mn(HCOO)_3$ were calculated on the basis of density functional theory calculations by employing the frozen-core projector augmented wave method [28,29] encoded in the Vienna Ab initio Simulation Package [30] with the generalized-gradient approximation for the exchange-correlation functional [31], a plane-wave cutoff energy of 520 eV, and 76 k points for the irreducible Brillouin zone. To describe the strong electron correlation at the magnetic site, the on-site repulsion $U_{eff} = U - J = 4$ eV was added on Mn^{2+} [32]. Spin-density distributions were calculated for the antiferromagnetic and ferromagnetic states of $[(CH_3)_2NH_2]Mn(HCOO)_3$ using the XCrySDen program [33].

III. RESULTS AND DISCUSSION

Figure 2(a) displays the magnetization of $[(CH_3)_2NH_2]Mn(HCOO)_3$ at temperatures above and below T_N. Field pulses up to 65 T reveal two low-temperature magnetically driven transitions. In addition to the spin-flop transition at $B_{SF} = 0.31$ T, we find a field-induced transition to the fully polarized state at $B_{Sat} = 15.3$ T. Using a magnetization of $0.66\mu_B$ at 2.08 K and 2 T, we find that the saturation magnetization is $5.2\mu_B$. Similar transitions to the saturated state occur in other materials including $Mn[N(CN)_2]_2$ and $MnCl_2(urea)_2$ [25,26]. The linear character of $M(B)$ between B_{SF} and B_{Sat} is in line with expectations for a three-dimensional system [7].

In our analysis of the magnetization and exchange interactions, we employ the experimentally determined saturation field ($B_{Sat} = 15.3$ T) and the spin Hamiltonian

$$H = -ZJ \sum_{\langle i,j \rangle_{xy}} S_i S_j - g\mu_B B \sum_i S_i^z, \qquad (1)$$

where Z is the coordination number of the Mn^{2+} center, $S = 5/2$, $g = 2.0$, and μ_B is the Bohr magneton. We extract $J = -0.69$ K [34]. This value compares well with that estimated from the zero-field susceptibility (−0.64 K) [13], although the absence of adjustable fit parameters makes it much less ambiguous [35]. The overall low energy scale of the exchange interactions explains why the spins can be saturated in experimentally realizable fields. Above T_N, magnetization increases gradually toward saturation. The general shape of $M(B)$ is evolving, but $M(B)$ does not turn into a Brillouin function above T_N. The spin-flop transition is no longer apparent, and the sharp knee denoting B_{Sat} is rounded due to the loss of long-range order. The gradual rise indicates that there are important short-range interactions above T_N. This is discussed in detail below.

Figure 2(b) displays the calculated spin density of $[(CH_3)_2NH_2]Mn(HCOO)_3$ in the antiferromagnetic and ferromagnetic states. In the zero-field (antiferromagnetic) state, spin density resides primarily on the Mn^{2+} centers and to a lesser extent on the formate ligand. The carbon center in each formate group is the node between the up- and down-spin states. In the $B \geqslant B_{Sat}$ (ferromagnetic) state, the spin-density pattern on Mn^{2+} and formate is similar although with an overall

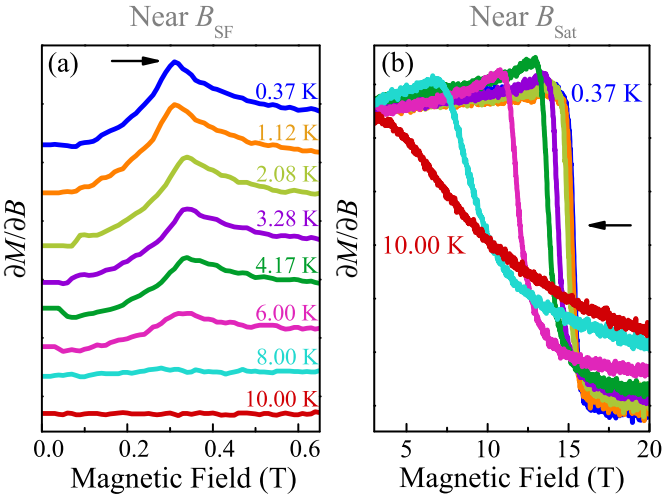

FIG. 3. (a) Closeup view of the derivative of the magnetization at different measurement temperatures in the vicinity of the spin-flop transition. The arrow denotes the position of the spin flop. (b) Derivative of the magnetization in the vicinity of the magnetic-driven phase transition. The arrow denotes the midpoint of the maximum slope, which defines the saturation field.

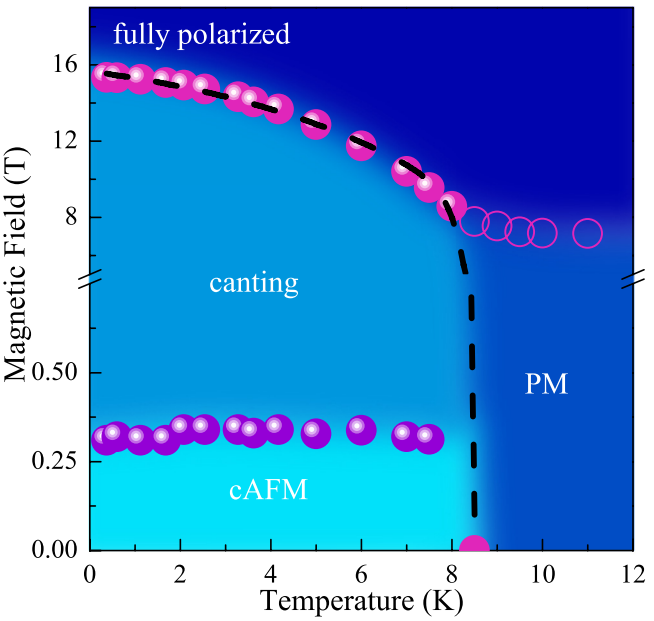

FIG. 4. B-T phase diagram of $[(CH_3)_2NH_2]Mn(HCOO)_3$ obtained from an analysis of pulsed field magnetization. PM = paramagnetic, cAFM = canted antiferromagnet. Closed circles correspond to boundaries involving long-range order. Open circles denote the region of short-range magnetic order. The 8.5-K Néel temperature is taken from Ref. [13]. Pulses up to 65 T reveal no additional features.

in-phase (rather than out-of-phase) arrangement. The node still resides on the carbon center in each formate group. This reflects participation of the nonbonding π level of $HCOO^-$ in the magnetic orbitals of the high-spin Mn^{2+}, which has no contribution from the carbon atom.

We carried out pulsed field magnetization shots at numerous temperatures in order to track the behavior of the 0.31 T spin flop and 15.3 T saturation transitions. Plots of $(\partial M/\partial B)_T$ vs B reveal inflection points that define these phase boundaries. In the former case, the peak locations define the position of B_{SF} whereas in the latter case, the region of maximum slope [36] defines B_{Sat}. Figure 3 summarizes the trends, and the arrows denote these positions. The signature of the spin-flop transition is subtle in the absolute magnetization [Fig. 2(a), inset], but it becomes apparent in the derivative plots. The strength of the feature (B_{SF}) diminishes with increasing temperature until it is no longer evident above T_N. The transition to the fully polarized state (B_{Sat}) is sharp at 0.37 K, and with increasing temperature, it broadens and shifts to lower fields. Trends below and above T_N represent the contributions of long-range magnetic order vs short-range ordering, respectively. The latter manifests as a broad derivativelike structure rather than a sharp jump. Recent work on other magnetic materials reveals that short-range correlations can survive well above the ordering temperature—sometimes to a surprising extent [37–40]. In $[(CH_3)_2NH_2]Mn(HCOO)_3$, this suggests that the magnetic aspects of multiferroicity can persist to much higher temperatures than previously supposed and certainly much higher than $T_N = 8.5$ K [21].

Bringing these results together, we generated the magnetic field-temperature phase diagram of $[(CH_3)_2NH_2]Mn(HCOO)_3$ (Fig. 4). As expected from the derivative analysis of the magnetization, there are two main phase boundary lines. The spin-flop transition is relatively stable at $B_{SF} = 0.31$ T, disappearing completely at $T_N = 8.5$ K. Increasing field suppresses the quantum fluctuations of the canted antiferromagnetic state and drives into the fully saturated magnetic state. The limiting low-temperature value of this phase boundary is $B_{Sat} = 15.3$ T. Whether this is a true magnetic quantum phase transition or not depends upon the behavior as $T \to 0$ K [41]. In any case, this magnetically driven transition is strongly temperature dependent: at $T_N/2 = 4.2$ K, B_{Sat} drops by 11%, and at 7 K, B_{Sat} falls by 32%. Even so, there is a strong remnant of the long-range-ordered state (in the form of short-range interactions) above T_N. This is evidenced by the broad, sweeping magnetization curve that also saturates (above 55 T at 10.00 K) but without the sharp knee that characterizes the critical field. These effects are diagramed by the open circles in Fig. 4. Similar short-range effects appear in other antiferromagnets including $CrSiTe_3$, $SrMnO_3$, $TbInO_3$, and $Cu(pyz)_2HF_2BF_4$ [37–40].

The phase diagram of this molecule-based multiferroic is analogous to that of other quantum magnets like $Mn[N(CN)_2]_2$ and $MnCl_2(urea)_2$ [25,26,42] in that it contains only spin-flop and saturation fields, although in this system, we have not only an adaptable framework but also a mechanism for multiferroic behavior. Thus, as magnetic field drives across the spin-flop and saturation transitions, changes in electronic properties may become apparent. The simplicity of the phase diagram and the overall accessibility of the high-field phase makes $[(CH_3)_2NH_2]Mn(HCOO)_3$ amenable to in-depth exploration [43] compared to the rare earth manganites. The B-T phase diagrams of the latter tend to be much more complicated, with numerous competing phases, noncollinear spin structures, and eventual saturation at higher fields [23].

Finally, the unexpected trends in the high-temperature polarization of $[(CH_3)_2NH_2]Mn(HCOO)_3$ can be linked to the structure of the B-T phase diagram and in particular the 15.3 T saturation field. The heart of this puzzle is that dielectric polarization is enhanced by 22% in a 13 T magnetic field between 150 and 190 K [16]. These temperatures are well above the magnetic ordering transition. At the same time, fits to the susceptibility in the vicinity of the ferroelectric transition [16], our magnetization data above T_N which extends to 12 K (Fig. 4), and the sizable magnetoelectric coupling at elevated temperatures (up to 40 K) [21] indicate that short-range interactions are important, although the temperature range is more limited. Nuclear magnetic resonance measurements on the Zn analog, on the other hand, reveal that T_C itself is insensitive to magnetic field and that there is no ordering of the amine—at least up to 5 T [44]. That spin resides on the metal-organic framework is consistent with our spin-density calculations in Fig. 2(b) as well as recent magnetoinfrared and neutron-scattering work [43,45]. Taken together, these findings suggest that $[(CH_3)_2NH_2]Mn(HCOO)_3$ is sensitive to magnetic field above T_N due to a remnant of the saturation field. In the absence of thermal fluctuations (well into the canted antiferromagnetic state), it is likely that dielectric polarization will be greatly enhanced under magnetic field. High-field polarization measurements across B_{Sat} will be useful to test this supposition.

IV. CONCLUSION

In summary, we investigated the magnetically driven phase transitions in $[(CH_3)_2NH_2]Mn(HCOO)_3$, a building block for a flexible new family of multiferroic materials. Using pulsed field magnetization, we unveil two features: a spin flop at 0.31 T and a transition to the fully polarized magnetic state at 15.3 T. The latter is in excellent agreement with mean-field theory, and first-principles spin-density calculations reveal the microscopic character of the phases. Tracking these critical fields with temperature, we generate a magnetic field-temperature phase diagram, which we discuss in terms of emerging properties in the high-field phase and its overall simplicity compared to the rare earth manganites. Importantly, we can explore the complete phase diagram of $[(CH_3)_2NH_2]Mn(HCOO)_3$ at laboratory magnetic fields due to the overall low energy scales in this system. This work opens the door to exploration of the high-field properties, provides a likely mechanism for emerging properties, and motivates the study of polarization in high magnetic fields.

ACKNOWLEDGMENTS

Research at Tennessee is supported by the National Science Foundation (Grant No. DMR-1707846) and the Materials Research Fund at the University of Tennessee. N.S.D. gratefully acknowledges partial support through National Science Foundation Grant No. CHE 1464955 and the Florida State University Lawton Fund. A portion of this work was performed at the National High Magnetic Field Laboratory, which is supported by the National Science Foundation through Grant No. DMR-1157490 and the States of Florida and New Mexico. J.S. appreciates funding from Basic Energy Sciences, US Department of Energy FWP "Science in 100 T program".

[1] F. J. Morin, Phys. Rev. **78**, 819 (1950).
[2] I. S. Jacobs, J. Appl. Phys. **32**, 61S (1961).
[3] Y.-G. Huang, D.-Q. Yuan, L. Pan, F.-L. Jiang, M.-Y. Wu, X.-D Zhang, W. Wei, Q. Gao, J. Y. Lee, J. Li, and M.-C. Hong, Inorg. Chem. **46**, 9609 (2007).
[4] P. Chen, N. Lee, S. McGill, S.-W. Cheong, and J. L. Musfeldt, Phys. Rev. B **85**, 174413 (2012).
[5] M. O. Yokosuk, A. al-Wahish, S. Artyukhin, K. R. O'Neal, D. Mazumdar, P. Chen, J. Yang, Y. S. Oh, S. A. McGill, K. Haule, S.-W. Cheong, D. Vanderbilt, and J. L. Musfeldt, Phys. Rev. Lett. **117**, 147402 (2016).
[6] S. M. Wu, W. Zhang, A. KC, P. Borisov, J. E. Pearson, J. S. Jiang, D. Lederman, A. Hoffmann, and A. Bhattacharya, Phys. Rev. Lett. **116**, 097204 (2016).
[7] P. A. Goddard, J. Singleton, P. Sengupta, R. D. McDonald, T. Lancaster, S. J. Blundell, F. L. Pratt, S. Cox, N. Harrison, and J. L. Manson, New J. Phys. **10**, 083025 (2008).
[8] S. Nellutla, M. Pati, Y.-J. Jo, H. D. Zhou, B. H. Moon, D. M. Pajerowski, Y. Yoshida, J. A. Janik, L. Balicas, Y. Lee, M. W. Meisel, Y. Takano, C. R. Wiebe, and N. S. Dalal, Phys. Rev. B **81**, 064431 (2010).
[9] S. Ghannadzadeh, J. S. Möller, P. A. Goddard, T. Lanńcaster, F. Xiao, S. J. Blundell, A. Maisuradze, R. Khasanov, J. L. Manson, S. W. Tozer, D. Graf, and J. A. Schlueter, Phys. Rev. B **87**, 241102 (2013).
[10] Y. Tokura, S. Seki, and N. Nagaosa, Rep. Prog. Phys. **77**, 076501 (2014).
[11] J. W. Kim, S. Artyukhin, E. D. Mun, M. Jaime, N. Harrison, A. Hansen, J. J. Yang, Y. S. Oh, D. Vanderbilt, V. S. Zapf, and S.-W. Cheong, Phys. Rev. Lett. **115**, 137201 (2015).
[12] G. Radtkea, A. Saúl, H. A. Dabkowskad, M. B. Salamone, and M. Jaime, Proc. Natl. Acad. Sci. USA **112**, 1971 (2015).
[13] P. Jain, V. Ramachandran, R. J. Clark, H. D. Zhou, B. H. Toby, N. S. Dalal, H. W. Kroto, and A. K. Cheetham, J. Am. Chem. Soc. **131**, 13625 (2009).
[14] P. J. Baker, T. Lancaster, I. Franke, W. Hayes, S. J. Blundell, F. L. Pratt, P. Jain, Z.-M. Wang, and M. Kurmoo, Phys. Rev. B **82**, 012407 (2010).
[15] A. Stroppa, P. Jain, P. Barone, M. Marsman, J. M. Perez-Mato, A. K. Cheetham, H. W. Kroto, and S. Picozzi, Angew. Chem., Int. Ed. **50**, 5847 (2011).
[16] W. Wang, L. Q. Yan, J. Z. Cong, Y. L. Zhao, F. Wang, S. P. Shen, T. Zou, D. Zhang, S.-G. Wang, X.-F. Han, and Y. Sun, Sci. Rep. **3**, 2024 (2013).
[17] Y. Tian, A. Stroppa, Y. Chai, L. Yan, S. Wang, P. Barone, S. Picozzi, and Y. Sun, Sci. Rep. **4**, 6062 (2014).
[18] M. Maczka, A. Gągor, B. Macalik, A. Pikul, M. Ptak, and J. Hanuza, Inorg. Chem. **53**, 457 (2014).
[19] Y. Tian, W. Wang, Y. Chai, J. Cong, S. Shen, L. Yan, S. Wang, X. Han, and Y. Sun, Phys. Rev. Lett. **112**, 017202 (2014).

[20] X.-Y. Wang, L. Gan, S.-W. Zhang, and S. Gao, Inorg. Chem. **43**, 4615 (2004).
[21] P. Jain, A. Stroppa, D. Nabok, A. Marino, A. Rubano, D. Paparo, M. Matsubara, H. Nakotte, M. Fiebig, S. Picozzi, E. S. Choi, A. K. Cheetham, C. Draxl, N. S. Dalal, and V. S. Zapf, npj Quantum Mater. **1**, 16012 (2016).
[22] K. Vinod, C. S. Deepak, S. Sharma, D. Sornadurai, A. T. Satya, T. R. Ravindran, C. S. Sundar, and A. Bharathi, RSC Adv. **5**, 37818 (2015).
[23] B. Lorenz, Condens. Matter Phys. **23**, 497073 (2013).
[24] L. Xin, Z. Fan, G. Li, M. Zhang, Y. Han, J. Wang, K. P. Ong, L. Qin, Y. Zheng, and X. Lou, New J. Chem. **41**, 151 (2017).
[25] T. V. Brinzari, P. Chen, Q.-C. Sun, J. Liu, L.-C. Tung, Y. Wang, J. A. Schlueter, J. Singleton, J. L. Manson, M.-H. Whangbo, A. P. Litvinchuk, and J. L. Musfeldt, Phys. Rev. Lett. **110**, 237202 (2013).
[26] J. L. Manson, Q. Huang, C. M. Brown, J. W. Lynn, M. B. Stone, J. Singleton, and F. Xiao, Inorg. Chem. **54**, 11897 (2015).
[27] N. Abhyankar, M. Lee, M. Foley, E. S. Choi, G. Strouse, H. W. Kroto, and N. S. Dalal, Phys. Status Solidi RRL **10**, 600 (2016).
[28] P. E. Blöchl, Phys. Rev. B **50**, 17953 (1994).
[29] G. Kresse and D. Joubert, Phys. Rev. B **59**, 1758 (1999).
[30] G. Kresse and J. Furthmüller, Phys. Rev. B **54**, 11169 (1996).
[31] J. P. Perdew, K. Burke, and M. Ernzerhof, Phys. Rev. Lett. **77**, 3865 (1996).
[32] S. L. Dudarev, G. A. Botton, S. Y. Savrasov, C. J. Humphreys, and A. P. Sutton, Phys. Rev. B **57**, 1505 (1998).
[33] A. Kokalj, Comput. Mater. Sci. **28**, 155 (2003).
[34] T. V. Brinzari, J. T. Haraldsen, P. Chen, Q.-C. Sun, Y. Kim, L.-C. Tung, Y. Wang, A. P Litvinchuk, J. A. Schlueter, D. Smirnov, J. L. Manson, J. Singleton, and J. L. Musfeldt, Phys. Rev. Lett. **111**, 047202 (2013).
[35] J. Brambleby, J. L. Manson, P. A. Goddard, M. B. Stone, R. D. Johnson, P. Manuel, J. A. Villa, C. M. Brown, H. Lu, S. Chikara, V. Zapf, S. H. Lapidus, R. Scatena, P. Macchi, Y.-S Chen, L.-C. Wu, and J. Singleton, Phys. Rev. B **95**, 134435 (2017).
[36] The mid point on the linear portion of the curve was used to determined the transition field.
[37] J. L. Musfeldt, L. I. Vergara, T. V. Brinzari, C. Lee, L. C. Tung, J. Kang, Y. J. Wang, J. A. Schlueter, J. L. Manson, and M.-H. Whangbo, Phys. Rev. Lett. **103**, 157401 (2009).
[38] L. D. Casto, A. J. Clune, M. O. Yokosuk, J. L. Musfeldt, T. J. Williams, H. L. Zhuang, M.-W. Lin, K. Xiao, R. G. Hennig, B. C. Sales, and D. Mandrus, APL Mater. **3**, 041515 (2015).
[39] S. Kamba, V. Goian, V. Skoromets, J. Hejtmánek, V. Bovtun, M. Kempa, F. Borodavka, P. Vaněk, A. A. Belik, J. H. Lee, O. Pacherová, and K. M. Rabe, Phys. Rev. B **89**, 064308 (2014).
[40] P. Chen, B. S. Holinsworth, K. R. O'Neal, T. V. Brinzari, D. Mazumdar, C. V. Topping, X. Luo, S.-W. Cheong, J. Singleton, S. McGill, and J. L. Musfeldt, Phys. Rev. B **91**, 205130 (2015).
[41] P. Coleman and A. J. Schofield, Nature (London) **433**, 226 (2005).
[42] K. R. O'Neal, J. H. Lee, M. Kim, J. L. Manson, Z. Liu, and J. L. Musfeldt [Nat. Quant. Mater. (to be published)].
[43] K. D. Hughey, A. J. Clune, M. O. Yokosuk, A. al-Wahish, S. Fan, N. Abhyankar, H. Xiang, Z. Li, J. Singleton, N. Dalal, and J. L. Musfeldt (unpublished).
[44] N. Abhyankar, J. J. Kweon, M. Orio, S. Bertaina, M. Lee, E. S. Choi, R. Fu, and N. S. Dalal, J. Phys. Chem. C **121**, 6314 (2017).
[45] H. D. Duncan, M. T. Dove, D. A. Keen, and A. E. Phillips, Dalton Trans. **45**, 4380 (2016).